

Ultrafast Photoinduced Dynamics of Pigment Yellow 101: Fluorescence, Excited-State Intramolecular Proton Transfer, and Isomerization

Lisa Lorenz, Jürgen Plötner, Victor V. Matyilitsky, Andreas Dreuw,* and Josef Wachtveitl*

Institute of Physical and Theoretical Chemistry, Johann Wolfgang Goethe University, Max von Laue-Strasse 7, 60438 Frankfurt, Germany

Received: May 2, 2007; In Final Form: August 15, 2007

The ultrafast excited-state dynamics of the fluorescent pigment yellow 101 (P.Y.101) and the closely related 1,1'-naphthalazine, a nonfluorescent derivative that lacks the OH groups at the naphthyl rings, are studied combining femtosecond spectroscopy and high-level quantum chemical calculations. The observed ultrafast dynamics and the spectral signature of photoexcited 1,1'-naphthalazine can be consistently explained with a previously proposed mechanism, suggesting fluorescence quenching via an optically forbidden $n\pi^*$ state. In contrast, for a description of the excited-state dynamics of P.Y.101, the expected simple absorption/fluorescence model is not adequate. Instead, besides fluorescence as the main decay channel of the excited-state population, ultrafast excited-state intramolecular proton transfer (ESIPT) and isomerization processes have to be considered for a complete understanding of the complex subnanosecond dynamics. Combining experiment and theory, the following kinetic model is derived: upon photoexcitation a major part of the excited-state population decays via fluorescence from an enol-type isomer of P.Y.101, while a small part of the population undergoes ESIPT and fluoresces from a keto-type form. Furthermore, arguments are given that, to a minor extent, also trans-cis isomerization of the keto form takes place on the S_1 surface leading probably to a long-lived cis-keto form in the ground state. The remarkable photostability of this organic pigment is thus achieved by the interplay of different ultrafast nondestructive decay channels.

Introduction

2,2'-Dihydroxy-1,1'-naphthalazine also known as pigment yellow 101 (P.Y.101, Figure 1) is an organic fluorescent yellow bis-azomethine pigment, which has been known since 1899 and industrially produced for decades.¹ It is special among the commercially available organic pigments with respect to its bright fluorescence in the solid state, which, unlike other organic pigments, does not require a special medium.¹ Not only because of its bright yellow color, but also due to its high photostability which guarantees the color fastness, P.Y.101 is used as a commercial colorant. Fluorescence is lost completely when the hydroxy substituents at the naphthyl rings are not present or are substituted with methoxy groups.^{2,3}

Although P.Y.101 has been known for more than a hundred years, its unusual solid-state fluorescence properties have only recently been addressed in experimental and theoretical studies.^{2,3} Combining crystallography, steady-state spectroscopy, and quantum chemical calculations, it has been shown that the observed solid-state fluorescence of P.Y.101 is a conserved property of the individual pigment molecules. Furthermore, an explanation could be given on a molecular level, why derivatives of P.Y.101 do not fluoresce when the OH groups are not present. Even a mechanism of fluorescence quenching in these non-fluorescent derivatives has been suggested on the basis of time-dependent density functional theory calculations. It was proposed that the nonradiative deexcitation pathway proceeds via an energetically low-lying $n\pi^*$ state along a CNN bending motion of the central bis-azomethine structure. However, the proposed mechanism still awaited experimental verification.

* Corresponding authors. E-mail: wveitl@theochem.uni-frankfurt.de (J.W.); andreas.dreuw@theochem.uni-frankfurt.de (A.D.).

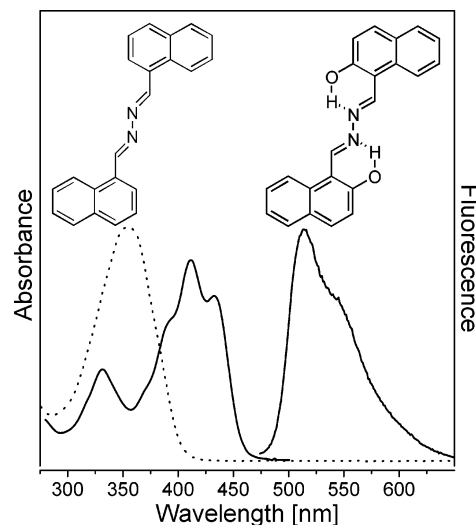


Figure 1. Steady-state absorption spectrum of 1,1'-naphthalazine (NA) (dotted line, molecular structure on the left) and absorption and fluorescence spectra of P.Y.101 (solid lines, molecular structure on the right).

Aromatic systems, which are structurally related to P.Y.101 and similarly exhibit intramolecular $N\cdots HO$ or $O\cdots HO$ hydrogen bonds, have already been extensively studied by time-resolved spectroscopy and/or theoretical approaches (refs 4–8 and references therein). In all these studies strong arguments have been given that excited-state intramolecular proton transfer (ESIPT) occurs, which in the studied systems corresponds to a keto–enol tautomerization on the excited-state potential energy surface. One example is 2,2'-hydroxybenzothiazol (HBT) that undergoes ESIPT upon excitation into its S_1 state within

approximately 50 fs.^{4,6} A similar time for ESIPT was found for 10-hydroxybenzoquinoline (10-HBQ), which is less flexible than HBT since both the proton donor and acceptor (the hydroxyl group and the nitrogen) are integrated into a quinoline moiety and thus fixed in a planar structure.⁷ In these studies ESIPT was assumed to proceed practically instantaneously as a ballistic wave packet motion. This process is driven by a low-frequency vibrational bending mode, which decreases the O–N distance and thus facilitates the ultrafast proton transfer leading from an enol to a keto structure in HBT.

To describe the dynamics and spectral signatures of ESIPT processes, typically four important structures need to be considered: the enol and keto isomers of the electronic ground and of the excited S_1 state, respectively. Typically the ESIPT process is described as follows: In nonpolar and non-hydrogen-donating solvents the enol ground-state structure is the predominant one at ambient conditions. Upon excitation into the optically allowed S_1 state, the proton is rapidly transferred from the donor to the acceptor group forming a keto-type structure. As a consequence, fluorescence is typically observed out of this keto isomer back to the ground state. Because the keto form is less stable than the enol form in the electronic ground state, the hydrogen is transferred back by thermal equilibration. Since the geometric changes are large on the S_1 potential energy surface for typical ESIPT systems, e.g., HBT and HBQ, large Stokes shifts of 7500 and 10000 cm^{-1} , respectively, are observed.

In our work, molecular spectroscopy and quantum chemical calculations are employed to obtain a detailed description of the ultrafast photoinduced dynamics of the bis-azomethine pigments P.Y.101 and 1,1'-naphthalazine (Figure 1), a derivative of P.Y.101 that lacks the hydroxy groups at the naphthyl rings. Steady-state absorption and fluorescence spectroscopy but, most importantly, femtosecond time-resolved transient absorption spectroscopy in the visible spectral range helped to get a detailed picture of ground and excited-state dynamics. Together with calculations at density functional theory (DFT) and time-dependent DFT (TDDFT) levels, a complete picture of the photoinduced subnanosecond dynamics of P.Y.101 and 1,1'-naphthalazine could be obtained. Whereas the nonfluorescent 1,1'-naphthalazine decays nonradiatively via a forbidden $n\pi^*$ state back to the ground state, P.Y.101 exhibits more complex excited-state dynamics. Although most of its excited-state population decays via fluorescence out of the enol form within some 10 ps, a small part of the population gives rise to longer-lived species. Arguments are given that these long-lived species result from isomerization processes leading to the formation of a long-lived cis-keto isomer in the ground state.

The comparison of the photoinduced dynamics of P.Y.101 and 1,1'-naphthalazine with the one of HBT and HBQ gives new insights into the mechanism of fluorescence quenching and ESIPT of aromatic molecules on the picosecond time scale.

Materials, Methods, and Computational Approach

Samples. The samples were provided by Clariant (Frankfurt Germany). They were synthesized by condensation of hydrazine with the corresponding naphthyl aldehydes.^{9–11} Dichloromethane (LiChrosolv) was obtained from Merck and used without further purification.

Steady-State Experiments. UV–vis spectra were recorded with a Specord S100 spectrophotometer from Analytik Jena. All steady-state measurements were performed with fused-silica cuvettes with 10 mm path length. Sample concentration in dichloromethane was 5 μM in the case of 1,1'-naphthalazine

and 3 μM for P.Y.101. The spectra were recorded versus the pure solvent. Fluorescence spectra were measured with a Varian Cary Eclipse fluorescence spectrophotometer. P.Y.101 and 1,1'-naphthalazine samples in dichloromethane were excited at the maximum of absorption (411 and 353 nm, respectively). The quantum yield of P.Y.101 has been determined from steady-state absorption and fluorescence measurements with coumarin 152 as reference.¹²

Time-Resolved Transient Spectroscopy. For time-resolved spectroscopy, sample concentration in dichloromethane was approximately 0.4 mM. The setup for transient pump–probe spectroscopy used for these measurements has been described in detail elsewhere.^{13,14} In brief, a Clark CPA 2001 femtosecond laser system operating at a repetition rate of 1 kHz and a central wavelength of 775 nm served as pulse source. Excitation pulses were generated by frequency doubling of the laser fundamental in a BBO crystal resulting in a pulse centered at 387 nm. The energy of the pump pulse was adjusted to 70 nJ. The sample was probed in a spectral range of 370–700 nm with single-filament white light pulses generated in a CaF_2 window. Because of group velocity mismatch between pump and probe light, the temporal resolution of the system is wavelength dependent. However, the cross correlation width for the entire investigated spectral range was not bigger than 150 fs. The continuum pulses were dispersed by two spectrometers (sample and reference) and recorded with two 42 segment diode arrays (multichannel detection), resulting in a spectral resolution of 8 nm. Data acquisition was performed in single-shot detection mode as balanced and referenced measurement providing signal-to-noise ratios up to 10^4 . The measurements were performed with fused-silica cuvettes with 1 mm path length. A two-dimensional movement of the sample cell was applied to provide nonexcited sample for successive laser shots. UV–vis absorption spectra were measured before and after the pump–probe experiments to control photoproduct formation and/or degradation of the samples.

After each femtosecond experiment, a measurement of the neat solvent under identical conditions was performed.

Data Analysis. Before further analysis, the data were corrected for the coherent signals and group velocity dispersion (GVD). The coherent signal of the solvent can be subtracted by the sample signal.¹⁵ The delay time zero was determined for all wavelengths employing a procedure described by Kovalenko et al.,¹⁶ which uses the temporal evolution of the coherent signal and a least-squares fit algorithm. Data were then analyzed using a Marquardt downhill algorithm that allows for simultaneous optimization of n exponential decays for all wavelengths, while the amplitudes for each kinetic component remain wavelength-dependent fitting parameters.

Computational Approach. The ground-state and excited-state geometries have been optimized with DFT^{17,18} and its time-dependent variant,^{19,20} respectively, employing the standard BP86^{21,22} exchange-correlation (xc) functional and the DZP²³ basis set as implemented in Turbomole 5.7 and Q-Chem 3.0.^{24–27} A previous study of xc-functional and basis set dependence revealed that the optimized geometries are practically independent of the chosen xc-functional/basis set combination.³ With increasing amount of Hartree–Fock exchange in the xc-functional, the excitation energies are shifted to higher absolute values, but most importantly, the order of the states does not change. We have chosen the BP86/DZP functional/basis set combination as standard in our computations. The absorption spectra are calculated at the equilibrium geometry of the electronic ground state, whereas the fluorescence spectra

are computed at the stationary points of the S_1 potential energy surface. All stationary points on the ground-state and excited-state surface have been checked by calculation of the harmonic frequencies. For the stationary points along the proton-transfer path obtained at the TDDFT level, RI-CC2²⁸ single-point calculations of the S_1 excitation energy have been performed employing the DZP basis set and SVP auxiliary fitting basis. The RI-CC2 results agree favorably with the ones obtained at the TDDFT level for the planar equilibrium structures. Most importantly, the order of the lowest excited states does not change.

Results

Steady-State Absorption and Fluorescence Spectra. Figure 1 shows the absorption and fluorescence spectra of 1,1'-naphthalazine (NA) and P.Y.101 in dichloromethane (DCM) solution at room temperature. NA exhibits only one absorption peak in the investigated spectral range of 200–1000 nm, which is centered at 354 nm. Under the chosen experimental conditions no steady-state fluorescence has been observed upon CW excitation of this band. Unlike NA, the absorption spectrum of P.Y.101 exhibits two bands at 340 and 411 nm. According to a previous, theoretical assignment, the band at 340 nm can most likely be attributed to the $S_0 \rightarrow S_3$ transition, the dominating latter one to the $S_0 \rightarrow S_1$ transition.³ The low-energy band exhibits a clear vibrational fine structure. In our previous theoretical analysis, it has been demonstrated that P.Y.101 possesses a corresponding symmetric stretch vibration of the bis-azomethine substructure at 1487 cm^{-1} at the theoretical level of TDDFT/BP86/DZP,^{2,3} which is most likely vibrationally excited, i.e., Franck–Condon active, upon photoexcitation.

Excitation of P.Y.101 at 411 nm, gives rise to the fluorescence spectrum depicted in Figure 1. The emission peak is found at 512 nm and shows a fine structure which is not a mirror image to the absorption, as it lacks the peak corresponding to the shoulder at 434 nm of the absorption spectrum. As indicated by the observed Stokes shift of 4800 cm^{-1} , the geometry of P.Y.101 has changed in the excited state compared to the geometry of the ground state, i.e., the Franck–Condon region. Indeed, the central bis-azomethine structure is transformed upon excitation from a $\text{C}=\text{N}-\text{N}=\text{C}$ into a $\text{C}\cdots\text{N}\cdots\text{N}\cdots\text{C}$ fragment.^{2,3} Note that the structurally related molecules HBT and 10-HBQ mentioned above exhibit significantly larger Stokes shifts of 7500 and $10\,000\text{ cm}^{-1}$, respectively, which were attributed to the formation of the keto tautomer via excited-state intramolecular proton transfer. Therefore, the main fluorescence peak observed at 512 nm for P.Y.101 does most likely not stem from fluorescence out of a keto-type structure but from fluorescence out of a local enol-type minimum of P.Y.101 in the excited S_1 state. This is also corroborated by our calculations, which will be discussed in detail later. The fluorescence quantum yield of P.Y.101 determined from steady-state measurements is in the order of 10^{-2} in DCM solution.

Although solvent effects go beyond the scope of this paper, it should be mentioned that an additional peak appears in the absorption spectrum at 520 nm, when P.Y.101 is dissolved in dimethyl sulfoxide (DMSO). This may be either due to the stabilization of the keto ground-state conformation or the deprotonation of the enol resulting in an enolate. The latter appears more likely, since according to our calculations the keto form is expected to absorb at 450 nm, whereas the enolate anion exhibits a stronger red-shift. Also in the fluorescence spectrum a second fluorescence band (centered at 620 nm) has been observed, which corroborates the formation of a new (probably

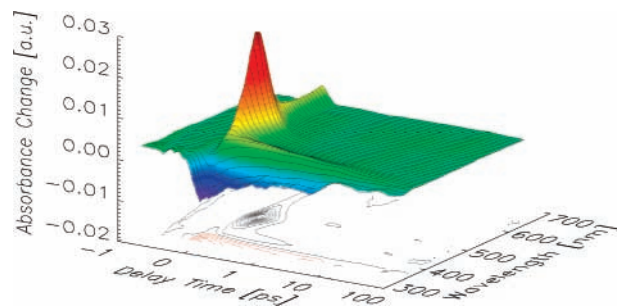


Figure 2. Transient absorption data of 1,1'-naphthalazine (NA) in dichloromethane after excitation at 387 nm. The time scale is plotted linear from -1 to 1 ps and logarithmic thereafter. Contours at the bottom illustrate the temporal evolution at different spectral ranges. Negative (blue) signals correspond to ground-state bleach, while positive (yellow and red) signals reflect excited-state absorption.

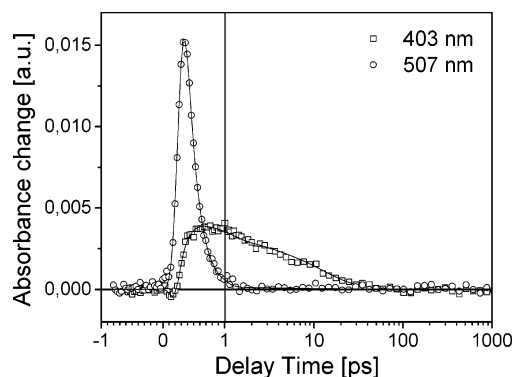


Figure 3. Transient absorbance changes of 1,1'-naphthalazine (NA) at 403 and 507 nm. Open symbols are experimental data points; the straight lines are the result of a multiexponential global fit analysis of the complete data set.

charged) species. A detailed investigation of the influence of the solvent on the optical properties of the bis-azomethine pigments shall be topic of further research.

Femtosecond Time-Resolved Spectroscopy of 1,1'-Naphthalazine and Pigment Yellow 101. Transient absorption changes of NA and P.Y.101 in DCM after excitation with 150 fs light pulses centered at a wavelength of 387 nm were recorded in a spectral range from 350 to 700 nm. In Figure 2, a complete set of the transient absorption data of NA is depicted. The plot shows the spectral and temporal evolution upon excitation at 387 nm from -1 to 100 ps. The spectrum is dominated by a strong, short-lived positive signal centered at 507 nm. Longer-lived contributions are found at shorter wavelengths: the negative (blue) contribution stems from the depletion of the ground state and comes along with a similarly intense excited-state absorption (ESA) which is centered around 400 nm. A spectrally broad, featureless contribution which is very short-lived is observed for wavelengths longer than 550 nm.

The individual lifetimes of the different components are seen more clearly in the transients (Figure 3), where the temporal behavior at selected probing wavelengths (λ_{pr}) is shown: the instantaneous increase in absorption, observed at $\lambda_{\text{pr}} = 507\text{ nm}$, decays completely within the first picosecond, whereas a long-lasting absorption increase is observed at $\lambda_{\text{pr}} = 403\text{ nm}$, which persists for more than 10 ps. The initial rise time of this transient is delayed compared to the 507 nm curve, due to a compensation of the initial ground-state bleach by the dominating ESA. After ca. 500 fs the maximum amplitude is reached at 403 nm, and the absorption decreases within 100 ps.

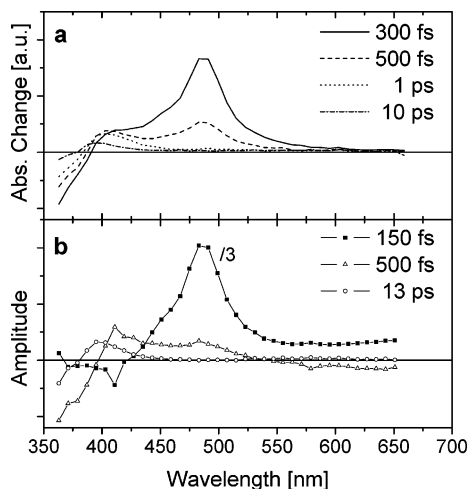


Figure 4. (a) Transient spectra of 1,1'-naphthalazine (NA) at selected delay times. (b) Decay-associated spectra of NA obtained from a global analysis. For an improved representation, the amplitude of the dominant 150 fs component was decreased by a factor of 3. The symbols correspond to data points, which are connected by straight lines to guide the eye.

Combining all transients and plotting their values at specific delay times leads to the transient spectra displayed in Figure 4a. They give an impression of the drastic wavelength dependence of the decay kinetics, where the gradual interconversion of the individual contributions can be observed. Comparing the spectrum after 300 fs delay time with the spectrum after 500 fs, a slight increase of the absorption change at 403 nm can be observed, whereas the signal around 480 nm is drastically decreased within this period of time. Within 1 ps the absorption in this spectral region disappears completely. Between 1 and 10 ps delay time, a spectral shift of the ESA signal from 410 to 400 nm can be observed.

For a proper description of the photoinduced excited-state kinetics, a minimum of three monoexponential functions are necessary. The procedure yields time constants of 150 fs, 500 fs, and 13.3 ps corresponding to the lifetimes of the intermediates. The amplitude spectra corresponding to the time constants are depicted in Figure 4b. The most drastic absorption change occurs on a short time scale ($\tau_1 = 150$ fs): The dominating part of the excited-state absorption (centered at 507 nm) decays mainly with a single-exponential kinetic (monophasic). However, this decay is interestingly not accompanied by a significant contribution to the recovery of the ground state ($\lambda < 400$ nm). Instead, the decay of the ESA signal might rather reflect the population of a lower lying excited state.

The remaining ESA decays biphasically with lifetimes of $\tau_2 = 500$ fs and $\tau_3 = 13.3$ ps and undergoes a slight blue-shift from 410 to 400 nm. The amplitude spectrum corresponding to τ_2 has a large negative contribution below 400 nm, indicating the recovery of the ground state, which further proceeds with τ_3 . Within 50 ps the ground-state recovery is completed.

Turning to the fluorescent pigment P.Y.101 one would naively expect a rather simple excited-state dynamics, i.e., absorption followed by fluorescence. Surprisingly, P.Y.101 exhibits a rather complicated excited-state dynamics, which is immediately evident from the time-resolved data (Figure 5). Its dynamic behavior is also substantially different from the one observed for NA, which is clear from the comparison of the respective three-dimensional (3D) data plots (Figures 5 and 2): all excited-state processes of P.Y.101 are more red-shifted, longer lived, and more complex than the ones of NA. The 3D plot of P.Y.101 (Figure 5) reveals three dominant characteristics: the ground-

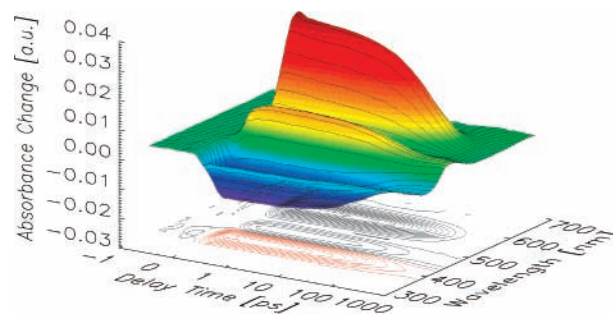


Figure 5. Transient absorption data of P.Y.101 in dichloromethane after excitation at 387 nm. Negative (blue) signals correspond to a bleach of the ground-state absorption, while positive signals (yellow and red) reflect excited-state absorption of the transient species.

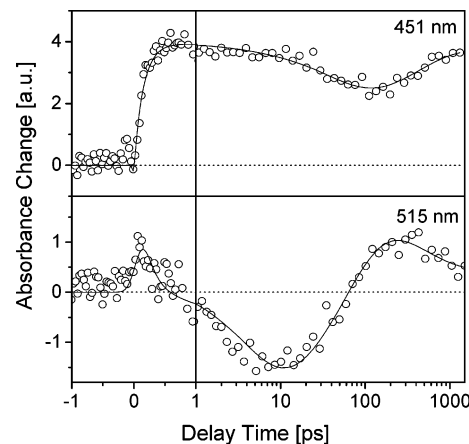


Figure 6. Transient absorbance changes of P.Y.101 at two characteristic wavelengths (451 and 515 nm). Open symbols are experimental data points; the straight lines are the result of a multiexponential global fit analysis of the complete data set.

state bleach, which is visible up to 460 nm (negative, blue), the excited-state absorption (positive, red), and a contribution from stimulated emission (SE) that is seen as a gap between two maxima of excited-state absorption. The SE signal (centered at 510 nm) divides the ESA into two parts. These findings are in good agreement with a system that absorbs light and relaxes due to stimulated emission. More complicated and unexpected is the fact that the system does not fully relax within the time of observation. After 1 ns a positive signal centered at 455 nm remains along with a ground-state bleach contribution. The positive and negative contributions are almost equal in intensity, indicating that the remaining signals are caused by the formation of a photoproduct or a long-lived intermediate.

The temporal behavior of the absorption changes is depicted in Figure 7a at different delay times. Comparing the first two spectra, corresponding to delay times of 0.2 and 3 ps, an ESA decrease can be observed, as well as a slight absorption increase around 480 nm. For longer delay times the trend of absorption decrease proceeds, together with the repopulation of the ground state. Comparing the spectra at 65 and 500 ps, the blue-shift of ESA from 480 to 460 nm can be seen. At 500 ps the absorption of the main ESA contribution has vanished, and the remaining signals around 470 and 420 nm persist almost unchanged throughout the remaining temporal range investigated (1.5 ns).

Isosbestic points, characteristic features of "two-level systems", are not clearly developed, although indicated at 450 and 510 nm in Figure 7a. Since the dominant contributions compensate each other at these spectral positions, these wavelengths are especially well suited for the observation of weaker components. The kinetic behavior at these wavelengths is

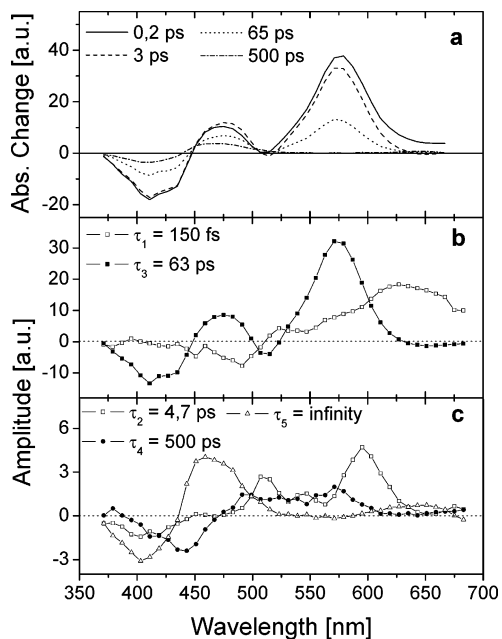


Figure 7. (a) Transient spectra of P.Y.101 at selected delay times. (b) Decay-associated spectra of P.Y.101 for dominant time constants, obtained from a global fitting analysis that was performed with five exponentials. (c) Decay-associated spectra for time constants with smaller amplitude.

depicted in Figure 6. The 451 nm transient shows a growing absorption after 100 ps, indicating that the delayed contribution from the photoproduct overlaps the initial ESA. At 515 nm the amplitude is close to zero, but again, signals from different contributions compete, giving rise to a small negative amplitude which reaches its minimum at 10 ps and can be assigned to stimulated emission occurring with this time constant. At later delay times, the signal increases again and finally leads to a positive amplitude after $\tau_D = 70$ ps.

To quantify these findings a global fitting routine has been performed. The data have been fitted with a set of four exponential decay times and a long-lived time constant ($\gg 1$ ns) accounting for the residual signal. Reconstruction of the data with the received decay times and amplitudes from the global fitting procedure are shown in Figure 6 (straight lines). The amplitude spectra for the different decay times are depicted in Figure 7, parts b and c. Two time constants ($\tau_1 = 150$ fs and $\tau_3 = 63$ ps) are clearly dominating and depicted in Figure 7b; the three spectra with smaller amplitude ($\tau_2 = 4.7$ ps, $\tau_4 = 500$ ps, and $\tau_5 = \text{infinity}$) are shown below (Figure 7c). The amplitude spectrum of the time constant $\tau_1 = 150$ fs shows no significant contributions below 450 nm, i.e., it contains no component contributing to the recovery of the ground state. The positive amplitude above 500 nm corresponds to the broad ESA which is narrowing on the fast time scale. The negative amplitude between 450 and 500 nm indicates the growing absorption that can be seen in the spectra on top at delay times of 0.2–3 ps.

The 4.7 ps time constant (τ_2) is rather low in amplitude, but here a contribution to the recovery of the ground state is found. The positive amplitude between 450 and 600 nm has two distinct maxima. In between a gap is found that spectrally corresponds to the shoulder of the fluorescence signal at 570 nm. It is likely that this gap is caused by stimulated emission from a local minimum on the S_1 surface, as will be discussed below.

The dominating kinetic feature of the system is described by the time constant $\tau_3 = 63$ ps, which has by far the largest

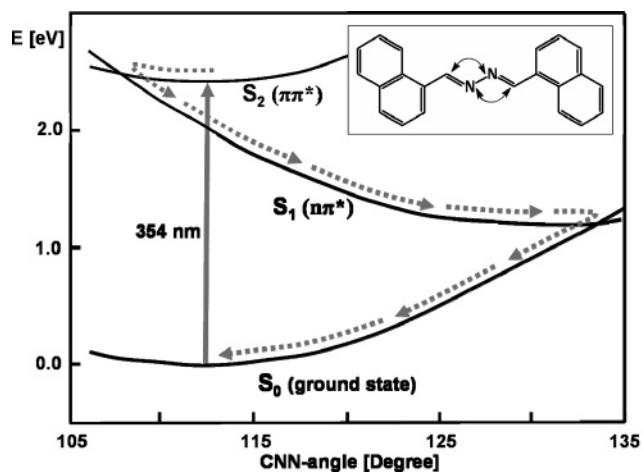


Figure 8. Nonradiative decay pathway for optically excited 1,1'-naphthalazine (NA) molecules along a CNN bending motion as calculated at the theoretical level of TDDFT.

amplitude: both the ESA and the ground-state bleach decrease on this time scale. The negative dip around 510 nm exactly matches the maximum of the fluorescence signal (Figure 1) and can thus be assigned to stimulated emission occurring with this time constant.

The time constant $\tau_4 = 500$ ps mainly reflects the blue-shift of the ESA, which most likely results from photoproduct formation. This kinetic component is most evident around 450 nm where it can be seen as the growing absorption for $\tau_D > 100$ ps (Figure 6).

Excited-State Properties and Geometries of 1,1'-Naphthalazine and Pigment Yellow 101. Theoretical investigation of the static optical properties of NA using TDDFT with the standard Becke–Perdew–1986 (BP86) exchange–correlation functional and the DZP basis set revealed that this pigment possesses a forbidden $n\pi^*$ S_1 state below the optically allowed $\pi\pi^*$ S_2 state.^{2,3} Furthermore, a potential fluorescence quenching mechanism was found for NA that proceeds from S_2 via S_1 back to the electronic ground state mediated by two curve crossings along a CNN bending motion of the central bis-azomethine subunit. The first crossing between S_2 and S_1 occurs close to the Franck–Condon region at a CNN angle of approximately 108° , while the second crossing is present between S_1 and S_0 at a CNN angle of about 133° bringing the excited-state population finally back to the electronic ground state (Figure 8). On the basis of simple geometric arguments, it is clear that the CNN bending motion is strongly coupled to the Franck–Condon active symmetric stretch mode of the central bis-azomethine subunit. Thus, the described bending motion provides an efficient nonradiative decay pathway for the excited-state population.

Also the static absorption and fluorescence spectra of P.Y.101 have previously been calculated using TDDFT/BP86/DZP, and it was shown that they agree favorably with the experimental spectra. At this level of theory, the energetically lowest excited S_1 state in P.Y.101 is an allowed $\pi\pi^*$ state absorbing at 510 nm at the ground-state equilibrium structure **A** and fluorescing at 589 nm at the planar equilibrium structure **B** (Figure 9) of the S_1 state (Table 1 and Figure 10). Comparison of the calculated absorption spectrum with the experimental one revealed that the theoretical spectrum is consistently red-shifted by ca. 0.6 eV corresponding to 100 nm for the main experimental absorption peak at 411 nm, which is typical for TDDFT calculations using the BP86 xc-functional. Thus, for interpretation purposes, all calculated absorption and fluorescence energies

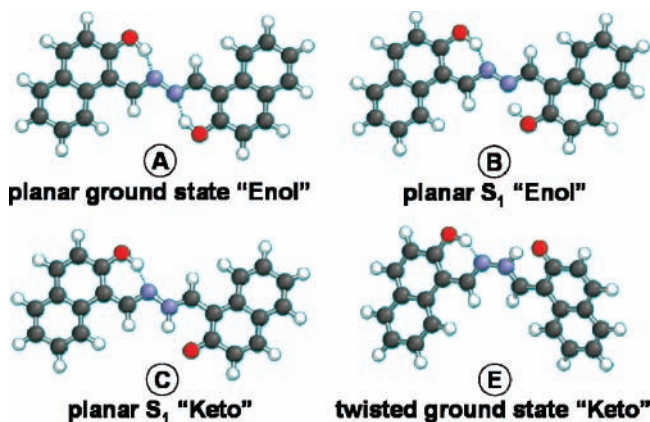


Figure 9. Ground- and excited-state equilibrium structures of P.Y.101 optimized at DFT/BP86/DZP and TDDFT/BP86/DZP levels of theory, respectively.

TABLE 1: Calculated, Shifted Calculated, and Experimental Absorption/Fluorescence Excitation Energies Ω [eV] (Oscillator Strengths) and Corresponding Excitation Wavelengths λ [nm] of the Ground-State trans-Enol Isomer A, the Planar Enol S_1 Isomer B, the Planar Keto Structure C, and the Ground-State cis-Keto Isomer E

structure	calcd abs./fl. TDDFT	shifted		exptl	
		Ω [eV]	λ [nm]	Ω [eV]	λ [nm]
A	2.44(0.69)	3.04	411	3.04	411
B	2.12(0.38)	2.72	459	2.43	512
C	1.88(0.27)	2.48	503	~ 2.3	~ 550
E	2.27(0.45)	2.87	435	~ 2.7	~ 460

have been shifted by 0.6 eV to the blue side of the spectrum (Table 1). After consideration of the shift (Table 1), the calculated and experimental excitation energies agree reasonably well, with errors of 0.2–0.3 eV.

For an explanation of the complicated photoinduced dynamics of P.Y.101 as described above, a previously assumed simple absorption/fluorescence model is not sufficient. For this objective, the potential energy surface (PES) of the S_1 state of P.Y.101 has been explored at the level of TDDFT/BP86/DZP to look for further nonradiative decay pathways accounting for the additional time constants. Since in related systems exhibiting intramolecular $N\cdots HO$ hydrogen bonds, e.g., HBT or HBQ (see the Introduction), ESIPT has been observed,^{4,6} we also checked for this possibility in P.Y.101. A cut through the PES of the ground and first excited state along the proton-transfer reaction path is displayed in Figure 10. Since the reaction coordinate essentially corresponds to the O–H distance, the OH bond is held fixed and the molecule is forced into a planar configuration in the calculation of the path while all other parameters were allowed to relax freely on the S_1 surface. Planarity had to be enforced, since otherwise the structure would relax into an artificial minimum on the S_1 surface at the employed TDDFT level of theory. This minimum corresponds to a twisted keto structure, in which the CNNC dihedral angle exhibits almost exactly 90° . This minimum is an artifact of TDDFT, since it possesses pronounced intramolecular charge transfer (CT) character indicated by its huge static electric dipole moment of 17 debye. It is today well documented that TDDFT systematically underestimates the excitation energies of excited CT states and thus, in our case, strongly favors the enolate form compared to the keto form.^{29,30} At the theoretical level of CIS (configuration interaction singles) not exhibiting the CT problem, the twisted enolate minimum disappears on the S_1 surface. Also, single-point RI-CC2 calculations reveal that the twisted keto isomer found by TDDFT lies significantly higher in energy than

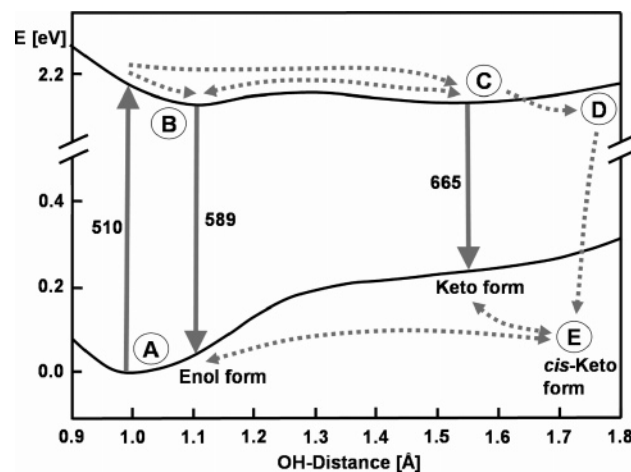


Figure 10. Calculated potential energy surfaces (PESs) of the ground and first excited state of P.Y.101 along the excited-state proton-transfer reaction coordinate, which is mainly represented by the O–H bond distance. Along the path, the O–H bond distance has been held fixed, while all other coordinates were allowed to relax freely on the S_1 surface. Solid up arrows correspond to absorption, solid down ones to fluorescence, and dashed arrows represent possible relaxation pathways. The additional decay paths from C to D and D to E indicate further possible nonradiative decay channels for C and D, which have been observed experimentally but not yet unambiguously identified theoretically.

the planar structures by 0.5 eV (12 kcal/mol). For the planar geometries, i.e., the optimized planar enol and keto structures A, B, and C (Figure 9), the agreement between RI-CC2 and TDDFT/BP86 is reasonable, but most importantly, the nature and the order of the lowest excited states are identical in both calculations. For example, the excitation energies for the TDDFT-optimized enol and keto forms are at the TDDFT/BP86 level 2.44 and 2.12 eV, whereas RI-CC2 yields 2.86 and 2.59 eV with a constant blue-shift of 0.4 eV.

However, our calculations clearly reveal that a planar keto equilibrium structure C (Figure 9) exists for P.Y.101, which lies 0.25 kcal/mol higher than B and is separated by a small energy barrier of 0.59 kcal/mol going from B to C (Figure 10). At the planar keto structure C, P.Y.101 exhibits a fluorescence wavelength of 665 nm at TDDFT/BP86/DZP level corresponding to a shifted wavelength of 503 nm (Table 1). The transfer of a second hydrogen atom resulting in a diketone is unlikely, since the corresponding structure lies 1.4 kcal/mol above the S_1 minimum B, and shall thus not be discussed further here.

A search for long-lived isomers of P.Y.101 on the ground-state PES revealed a stable twisted keto isomer E (Figure 9), in which the CNNC angle exhibits a value of 30.4° , which corresponds essentially to a cis configuration of the central bis-azomethine subunit, in contrast to the originally planar trans configuration of the initial enol structure A. Energetically, isomer E is 8.9 kcal/mol higher in energy than isomer A, but a significant energy barrier of typically 5 kcal/mol has to be passed to thermally return from E to A on the ground-state surface. Furthermore, this isomer exhibits a 48 nm red-shifted absorption wavelength of 549 nm compared to the global enol minimum at TDDFT level, corresponding to a shifted value of 460 nm.

Ultrafast Excited-State Dynamics of 1,1'-Naphthalazine and Pigment Yellow 101. Combining our experimental and theoretical findings, we arrive at the following kinetic model for the ultrafast excited-state dynamics of NA. Photoexcitation of NA with 387 nm laser pulses results in the population of the $\pi\pi^*$ excited S_2 state (Figure 8). This excited-state population is seen in our pump–probe experiment as broad spectral excited-

state absorption between 400 and 600 nm (Figures 2 and 4), which decays very rapidly with a time constant of 150 fs. The corresponding amplitude spectrum does not exhibit any contribution to the recovery of the ground-state bleach, but contains a negative amplitude around 400 nm, representing the population of another state absorbing stronger in the blue spectral range (Figure 4b). The latter state can be identified as an $n\pi^*$ excited S_1 state, which according to our computations exhibits no oscillator strength and is thus not seen in the static absorption spectrum. Also, the delayed rise time of the positive signal in the transient spectrum at 403 nm is due to S_1 population: upon its formation the S_1 ESA gradually overcomes the instantaneous ground-state bleach, which clearly shows that this state is not populated instantaneously. The fast time scale of the nonradiative $S_2 \rightarrow S_1$ transition corroborates the existence of the previously theoretically identified S_2/S_1 crossing along a CNN bending mode (Figure 8). The S_1 population decays then within 1 ps as indicated by the corresponding amplitude spectrum ($\tau_1 = 150$ fs). Moreover, the strong negative amplitude between 350 and 400 nm indicates a strong contribution to the ground-state recovery, i.e., the S_1 state decays into the ground state. Thus, it is possible for the S_2 population to decay very quickly within a few vibrations back into the ground state via the two S_2/S_1 and S_1/S_0 state crossings. In addition to these fast decay components, a slower 13 ps time constant is also necessary to describe the excited-state dynamics in the pump–probe experiment. However, the corresponding amplitude spectrum is very similar to the one of the 500 fs component, also contributing to the ground-state recovery (Figure 4b). This contribution can thus most likely be explained as a part of the S_1 excited-state population that misses the S_1/S_0 crossing and remains longer in the excited S_1 state. The experimental and theoretical results clearly demonstrate the mechanism of fluorescence quenching in NA via two excited-state crossings along a CNN bending motion (Figure 8).

Turning to the fluorescent P.Y.101, our pump–probe experiments revealed that its excited-state dynamics is much more complex than the anticipated simple absorption/fluorescence scheme. However, a combined analysis of the TA experiments and the theoretical findings yields the following kinetic model for the ultrafast excited-state dynamics of P.Y.101 (Figure 10). Upon excitation, the excited-state population of the optically allowed S_1 state moves out of the Franck–Condon region **A** and populates both the planar enol (**B**) and planar keto (**C**) structures of the S_1 state. With the 150 fs time constant the red part of the ESA vanishes, and absorption grows between 450 and 520 nm (negative signal, Figure 7b). This means a particular molecular conformation is adopted which absorbs in this spectral range.

Since the enol form **B** corresponds to a local minimum on the S_1 PES, that part of the population that is caught in this minimum will decay via fluorescence with the 63 ps time constant. The amplitude spectra reveal that this is the dominating process. Thus, fluorescence from the enol conformation represents the main deactivation channel of P.Y.101. With the dissipation of the excess energy, a transition from **B** to **C** or **D** becomes unlikely, since they are separated by energy barriers. Also, the planar keto structure **C** corresponds to a local minimum, but it is found to lie 0.25 kcal/mol energetically above the enol minimum. Since the excited-state population of **C** can decay either back to the enol isomer **B** or to conformer **D** or via fluorescence, the lifetime of the population of **C** can be assumed to be shorter than the one of **B**. These theoretical findings are in agreement with the amplitude spectra of the

4.7 ps component, which we assign to depopulation of **C**. The gap in the amplitude spectrum around 570 nm indicates that in this region fluorescence and ESA compete.

With these findings the steady-state fluorescence signal (Figure 1) can be consistently explained by dual fluorescence: The main peak centered at 507 nm and the shoulder at 540 nm most likely corresponds to the ($\nu'_0-\nu_2$ and $\nu'_0-\nu_1$) transition from the excited enol-like conformer to the enol ground state. The third contribution which broadens the spectrum can be assigned to fluorescence from the excited keto-like structure, proceeding with a time constant of 4.7 ps.

The amplitude spectrum of the $\tau_4 = 500$ ps component can be assigned to the lifetime of the unknown conformer **D**. The red part of the amplitude spectrum of τ_4 corresponds to the ESA from **D**, the negative contribution around 500 nm to ground-state recovery. This band is clearly red-shifted in comparison to the initial ground-state bleach, indicating the growing absorption of an additional isomer on the ground-state PES. Finally, the long-lived population with a lifetime exceeding the observation time of our experiment corresponds most likely to a cis-keto isomer **E** of the electronic ground state. There was no experimental evidence for the formation of a stable photo-product due to sample degradation. This cis-keto isomer is formed on the ground-state PES via **D** and exhibits a shifted calculated electronic absorption at approximately 434 nm, i.e., 25 nm red-shifted compared to the planar ground-state trans-enol isomer **A** (Figure 9). The amplitude spectrum of the long-lived component exhibits excited-state absorption around 460 nm and can thus be correlated with the theoretically identified cis-keto isomer **E**. The fact that the latter can return to the original trans-enol form **A** only via thermal isomerization explains the long lifetime of this conformer.

Since the cis-keto form originates from the decay of the unknown conformer **D**, one can guess the structure of **D**. Obviously, the latter must correspond to a keto-type structure on the S_1 surface exhibiting at least a pretwist around the central CNNC moiety. Unfortunately, due to the CT problem of TDDFT, it was not yet possible to unambiguously clarify whether **D** corresponds to a true cis-keto isomer similar to **E** or to a 90° twisted structure, but we believe that photoinitiated trans–cis isomerization in the keto-form also takes place on the S_1 PES.

In comparison with the structurally closely related molecules HBT and HBQ, which also undergo ESIPT, the excited-state dynamics of P.Y.101 is remarkably different. Whereas the excited-state populations in HBT and HBQ decay via fluorescence out of the keto-form, P.Y. 101 fluoresces mostly out of the enol-form, and only a small part of the excited-state population undergoes ESIPT. The different excited-state dynamics certainly have their origin in the different topology of their PESs. Most significantly, in HBT and HBQ, the keto isomers are found to be energetically lower than the corresponding enol form, which is the opposite in P.Y.101.

Summary and Conclusions

In this work a combination of advanced femtosecond pump–probe spectroscopy and quantum chemical calculations has been employed to study the complicated, ultrafast excited-state dynamics of two structurally closely related organic yellow pigments, 2,2'-dihydroxy-1,1'-naphthalazine also known as pigment yellow 101 (P.Y.101) and 1,1'-naphthalazine (NA). Despite the similarity of their molecular structures, their optical properties are remarkably different.

It has been demonstrated that the nonfluorescent yellow pigment 1,1'-naphthalazine possesses an optically forbidden $n\pi^*$

excited state as the energetically lowest excited state, which mediates efficient fluorescence quenching via two-state crossings between the optically excited S_2 and the S_1 state as well as between the S_1 and S_0 states along a CNN bending motion of the central bis-azomethine structure.

On the contrary, the fluorescent P.Y.101 is optically excited in its allowed $\pi\pi^*$ S_1 state suggesting a simple absorption/fluorescence excited-state dynamics. Surprisingly, pump-probe experiments revealed a complicated excited state subnanosecond dynamics of P.Y.101 with five time constants necessary for a description of the ongoing processes. It could be shown that ESIPT results in the formation of a keto-form of P.Y.101 on the S_1 surface and that most likely trans-cis isomerization of the central bis-azomethine subunit leads to a long-lived cis-keto ground-state structure. Nevertheless, fluorescence is the main decay path of the S_1 excited-state population, which occurs mostly out of the enol-form and only to a minor extent out of the keto-form of P.Y.101.

Our experiments have been performed in solution, although in technical applications P.Y.101 is typically used as microcrystals, due to its poor solubility in most solvents. In the crystal structure P.Y.101 is tightly packed, and the question arises, how crystallization affects the excited-state dynamics. In principle, one can expect that ESIPT also occurs in the crystal, since during this fast process P.Y.101 remains planar and no additional steric hindrance should occur. However, the isomerization process will probably be hindered by the tight crystal packing, since it requires a large-scale rotation around the central NN bond. At present, this remains uncertain and is thus subject to future research.

Another open question is the identification of conformer **D** on the S_1 surface of P.Y.101, which eventually leads to the formation of the ground-state cis-keto isomer. Here, we hope to get further insight from time-resolved infrared spectroscopy, which hopefully will reveal information on the structures of the individual conformers.

P.Y.101 is exploited in many technical applications, and despite its rather low fluorescence quantum yield in solution, it exhibits a remarkable photostability and color fastness. In general, a requirement for molecules to be photostable is that they exhibit only radiative and nonradiative decay channels that are nondestructive. In other words, photostable molecules must not undergo dissociation or other chemical reactions upon photoexcitation. For example, DNA has been shown to be photostable due to excited-state intermolecular hydrogen transfer between adjacent base pairs.^{31–33} The hydrogen transfer deactivates the base and after back-transfer of the hydrogen in the electronic ground state the original DNA base pair is recovered. From our combined experimental and theoretical study on P.Y.101 it is clear that all identified deactivation pathways, fluorescence out of the excited-state enol or keto forms, intramolecular proton transfer, and isomerization, are nondestructive in that they all lead back to the original planar enol structure of P.Y.101. Even the possible isomerization to the long-lived cis-keto form will eventually lead back to the planar enol isomer via thermal equilibration on the ground-state surface. This finally explains the exceptional photostability and color fastness of the organic P.Y.101.

Acknowledgment. The authors are indebted to Professor Martin U. Schmidt for introducing them to pigment yellow 101

and to Dr. T. Metz, Clariant GmbH, for providing the samples. A. Dreuw acknowledges financial support by the Deutsche Forschungsgemeinschaft as an Emmy-Noether fellow.

References and Notes

- (1) Herbst, W.; Hunger, K. *Industrial Organic Pigments*, 3rd ed.; Wiley-VCH: Weinheim, Germany, 2004.
- (2) Dreuw, A.; Plötner, A.; Lorenz, L.; Wachtveitl, J.; Djanhan, J. E.; Brüning, B.; Metz, T.; Bolte, M.; Schmidt, M. U. *Angew. Chem., Int. Ed.* **2005**, *44*, 7783.
- (3) Plötner, J.; Dreuw, A. *Phys. Chem. Chem. Phys.* **2006**, *8*, 1197.
- (4) de Vivie-Riedle, R.; De Waele, V.; Kurtz, L.; Riedle, E. *J. Phys. Chem. A* **2003**, *107*, 10591.
- (5) Lochbrunner, S.; Schultz, T.; Schmitt, M.; Shaffer, J. P.; Zgierski, M. Z.; Stolow, A. *J. Chem. Phys.* **2001**, *114*, 2519.
- (6) Lochbrunner, S.; Wurzer, A. J.; Riedle, E. *J. Phys. Chem. A* **2003**, *107*, 10580.
- (7) Takeuchi, S.; Tahara, T. *J. Phys. Chem. A* **2005**, *109*, 10199.
- (8) Sobolewski, A. L.; Domcke, W.; Hättig, C. *J. Phys. Chem. A* **2006**, *110*, 6301.
- (9) Blout, E. R.; Gofstein, R. M. *J. Am. Chem. Soc.* **1945**, *67*, 13.
- (10) Mathur, S. S.; Suschitzky, H. *J. Chem. Soc., Perkin Trans. 1* **1975**, 2479.
- (11) Shapiro, N. *Ber. Dtsch. Chem. Ges.* **1933**, *66*, 1103.
- (12) Williams, A. T. R.; Winfield, S. A.; Miller, J. N. *Analyst* **1983**, *108*, 1067.
- (13) Helbing, J.; Bregy, H.; Bredenbeck, J.; Pfister, R.; Hamm, P.; Huber, R.; Wachtveitl, J.; De Vico, L.; Olivucci, M. *J. Am. Chem. Soc.* **2004**, *126*, 8823.
- (14) Huber, R.; Köhler, T.; Lenz, M. O.; Bamberg, E.; Kalmbach, R.; Engelhard, M.; Wachtveitl, J. *Biochemistry* **2005**, *44*, 1800.
- (15) Lorenc, M.; Ziolk, M.; Naskrecki, R.; Karolczak, J.; Kubicki, J.; Maciejewski, A. *Appl. Phys. B: Lasers Opt.* **2002**, *74*, 19.
- (16) Kovalenko, S. A.; Dobryakov, A. L.; Ruthmann, J.; Ernsting, N. *P. Phys. Rev. A* **1999**, *59*, 2369–2384.
- (17) Parr, R. G.; Yang, W. *Density Functional Theory of Atoms and Molecules*; Oxford University Press: Oxford, 1989.
- (18) Parr, R. G.; Yang, W. *Annu. Rev. Phys. Chem.* **1995**, *46*, 701.
- (19) Dreuw, A.; Head-Gordon, M. *Chem. Rev.* **2005**, *105*, 4009.
- (20) Casida, M. E. In *Recent Advances in Density Functional Methods, Part I*; Chong, D. P., Ed.; World Scientific: Singapore, 1995.
- (21) Becke, A. D. *Phys. Rev. A* **1988**, *38*, 3098.
- (22) Perdew, J. P. *Phys. Rev. B* **1986**, *34*, 7406.
- (23) Dunning, T. H. *J. Chem. Phys.* **1970**, *53*, 2823.
- (24) Ahlrichs, R.; Bär, M.; Häser, M.; Horn, H.; Kolmel, C. *Chem. Phys. Lett.* **1989**, *162*, 165.
- (25) Häser, M.; Ahlrichs, R. *J. Comput. Chem.* **1989**, *10*, 104.
- (26) Weiss, H.; Ahlrichs, R.; Häser, M. *J. Chem. Phys.* **1993**, *99*, 1262.
- (27) Shao, Y.; Molnar, L. F.; Jung, Y.; Kussmann, J.; Ochsenfeld, C.; Brown, S. T.; Gilbert, A. T. B.; Slipchenko, L. V.; Levchenko, S. V.; O'Neill, D. P.; DiStasio, R. A., Jr.; Lochan, R. C.; Wang, T.; Beran, G. J. O.; Besley, N. A.; Herbert, J. M.; Lin, C. Y.; Van Voorhis, T.; Chien, S. H.; Sodt, A.; Steele, R. P.; Rassolov, V. A.; Maslen, P. E.; Korambath, P. P.; Adamson, R. D.; Austin, B.; Baker, J.; Byrd, E. F. C.; Dachsels, H.; Doerksen, R. J.; Dreuw, A.; Dunietz, B. D.; Dutoi, A. D.; Furlani, T. R.; Gwaltney, S. R.; Heyden, A.; Hirata, S.; Hsu, C.-P.; Kedziora, G.; Khalliulin, R. Z.; Klunzinger, P.; Lee, A. M.; Lee, M. S.; Liang, W. Z.; Lotan, T.; Nair, N.; Peters, B.; Proynov, E. I.; Pieniazek, P. A.; Rhee, Y. M.; Ritchie, J.; Rosta, E.; Sherrill, C. D.; Simmonett, A. C.; Subotnik, J. E.; Woodcock, H. L., III; Zhang, W.; Bell, A. T.; Chakraborty, A. K.; Chipman, D. M.; Keil, F. J.; Warshel, A.; Hehre, W. J.; Schaefer, H. F., III; Kong, J.; Krylov, A. I.; Gill, P. M. W.; Head-Gordon, M. *Phys. Chem. Chem. Phys.* **2006**, *8*, 3172.
- (28) Sobolewski, A. L.; Domcke, W.; Hättig, C. *J. Phys. Chem. A* **2006**, *110*, 6301.
- (29) Dreuw, A.; Head-Gordon, M. *J. Am. Chem. Soc.* **2004**, *126*, 4007.
- (30) Dreuw, A.; Weisman, J. L.; Head-Gordon, M. *J. Chem. Phys.* **2003**, *119*, 2943.
- (31) Perun, S.; Sobolewski, A. L.; Domcke, W. *J. Am. Chem. Soc.* **2005**, *127*, 6257.
- (32) Schultz, T.; Samoylova, E.; Radloff, W.; Hertel, I. V.; Sobolewski, A. L.; Domcke, W. *Science* **2004**, *306*, 1765.
- (33) Sobolewski, A. L.; Domcke, W.; Hättig, C. *Proc. Natl. Acad. Sci. U.S.A.* **2005**, *102*, 17903.